SPECIAL
DIMES
COLLECTION

Enhanced Diapycnal Diffusivity in Intrusive Regions of the Drake Passage

SOPHIA T. MERRIFIELD

Massachusetts Institute of Technology/Woods Hole Oceanographic Institution Joint Program, Woods Hole Oceanographic Institution, Woods Hole, Massachusetts

LOUIS ST. LAURENT AND BRECK OWENS

Department of Physical Oceanography, Woods Hole Oceanographic Institution, Woods Hole, Massachusetts

ANDREAS M. THURNHERR

Division of Ocean and Climate Physics, Lamont–Doherty Earth Observatory, Palisades, New York

JOHN M. TOOLE

Department of Physical Oceanography, Woods Hole Oceanographic Institution, Woods Hole, Massachusetts

(Manuscript received 7 April 2015, in final form 22 January 2016)

ABSTRACT

Direct measurements of oceanic turbulent parameters were taken upstream of and across Drake Passage, in the region of the Subantarctic and Polar Fronts. Values of turbulent kinetic energy dissipation rate ε estimated by microstructure are up to two orders of magnitude lower than previously published estimates in the upper 1000 m. Turbulence levels in Drake Passage are systematically higher than values upstream, regardless of season. The dissipation of thermal variance χ is enhanced at middepth throughout the surveys, with the highest values found in northern Drake Passage, where water mass variability is the most pronounced. Using the density ratio, evidence for double-diffusive instability is presented. Subject to double-diffusive physics, the estimates of diffusivity using the Osborn–Cox method are larger than ensemble statistics based on ε and the buoyancy frequency.

1. Introduction

A number of processes in the Southern Ocean are thought to support high levels of mixing relative to other regions of the global ocean. At the surface, strong winds and storms force the ocean at near-inertial frequencies, generating internal waves that can propagate downward (Price 1981). Upper-ocean and middepth values of diapycnal diffusivity are believed to be set in part by the breaking of these near-inertial waves (e.g., Wu et al. 2011). Deep-reaching currents associated with density fronts flow over rough topography, generating internal lee waves that radiate energy and provide power for turbulence in the stratified ocean interior (e.g., Nikurashin and Ferrari 2010). Water mass variability and strong mesoscale activity also precondition the water column for double-diffusive instability (e.g., Joyce et al. 1978).

Because of the remoteness and harsh conditions, few direct measurements of mixing have been made in the Southern Ocean. A growing body of work has used hydrographic and velocity finescale data to estimate diapycnal mixing rates in this region (Garabato et al. 2004; Thompson et al. 2007; Sloyan et al. 2010; Wu et al. 2011; Whalen et al. 2012). Thorpe-scale analysis (Thorpe 1977) and shear/strain-based methods (Kunze et al. 1990) are most commonly used to estimate microscale quantities. However, recent work has shown the potential for biases between mixing rates inferred from both of those methods and those from direct measurements. Mater et al. (2015) found Thorpe-scale methods overestimate mixing rates when compared to direct measurements,

Corresponding author address: Sophia T. Merrifield, MIT/WHOI Joint Program, Woods Hole Oceanographic Institution, 266 Woods Hole Rd., MS29, Woods Hole, MA 02543.
E-mail: stm@mit.edu

DOI: 10.1175/JPO-D-15-0068.1

especially in the presence of large overturns. In the Southern Ocean, mixing rates inferred from finescale parameterizations are shown to overestimate those from microstructure measurements by as much as one to two orders of magnitude (Frants et al. 2013).

Previous estimates of middepth mixing rates based on finescale methods have been linked to both surface and bottom-generated breaking internal waves. Garabato et al. (2004) attributed high values of diffusivity ($\kappa_\rho \sim 10^{-4}\,\mathrm{m^2\,s^{-1}}$ between 500 and 1000 m) to bottom-generated lee waves. Multiple studies (Wu et al. 2011; Sloyan et al. 2010; Thompson et al. 2007; Kilbourne and Girton 2014) suggest wind-excited near-inertial waves radiate into the interior and break, contributing to high values of mixing below the surface layer. However, direct evidence of this process is still lacking. From these estimates of mixing rates, spatial and temporal patterns have been inferred. Thompson et al. (2007) conclude that the regions north and south of the Polar Front (PF) are dynamically different. Wu et al. (2011) suggested that seasonality in the wind stress at the surface contributes to seasonality in mixing rates as deep as 1500 m. Because of finescale biases in mixing rates from previously published studies, there is a renewed need to discuss the patterns and dynamics using direct measurements in this region.

The role of double-diffusive instability in driving mixing in the Southern Ocean has not been addressed using microstructure measurements. Studies focusing on the intrusive water mass characteristics in this region suggested that double-diffusive instability could be important to the dynamics (Joyce et al. 1978; Toole and Georgi 1981; You 2002), but a comprehensive effort to study this using direct fine- and microstructure temperature T and salinity S has been missing. This work seeks to fill that gap by evaluating the density ratio $R_\rho = (\alpha\overline{T}_z)/(\beta\overline{S}_z)$, where α is the thermal expansion coefficient, β is the haline contraction coefficient, $\overline{S}_z$ is the mean vertical gradient of salinity, $\overline{T}_z$ is the mean vertical gradient of temperature, and R_ρ is a parameter that quantifies the favorability to double-diffusive instability. The two flavors of double-diffusive instability, salt fingering and diffusive convection, can occur when $1 < R_\rho < 100$ and $0 < R_\rho < 1$, respectively. A narrower range of this ratio results in a growth rate that allows the instability to develop on a time scale comparable to the local buoyancy period ($2\pi/N$). This range has been estimated to be $1 < R_\rho < 2$ for salt fingering and $0.5 < R_\rho < 1$ for diffusive convection (Schmitt 1979).

The Diapycnal and Isopycnal Mixing Experiment in the Southern Ocean (DIMES) has recorded more than 500 CTD and 200 microstructure profiles with heavy sampling in Drake Passage. The direct measurements of dissipation made as part of the DIMES study are described by Ledwell et al. (2011), St. Laurent et al. (2012), and Sheen et al. (2014). These studies showed that enhanced internal wave fine structure and turbulence levels were not widespread but were limited to frontal zones where strong bottom currents collide with significant topography. In particular, St. Laurent et al. (2012) showed that velocity fine- and microstructure characteristics above the Phoenix Ridge are consistent with internal lee waves. There, the signal of enhanced dissipation extended to heights of 1500 m above the local ridge topography.

Here we present direct measurements of dissipation to study middepth values of the turbulent kinetic energy dissipation rate ε and the dissipation of thermal variance χ. Values of dissipation are shown to be up to two orders of magnitude smaller than previously published values in the upper 1000 m inferred from finescale parameterizations. This work seeks to do the following:

1) report estimates of dissipation and diffusivity in the upper 1500 m of the Drake Passage region;
2) present evidence that double diffusion is a potentially important contributor to enhanced rates of thermal variance dissipation and vertical diffusivity; and
3) generate maps of the density ratio from hydrographic data to indicate regions of the Southern Ocean that may be susceptible to double-diffusive instability.

2. Observations

This study uses data from two field expeditions of the DIMES study, hereinafter referred to as the US2 and US5 expeditions (Fig. 1). Both expeditions originated and ended in Punta Arenas, Chile. US5 occupied a localized survey grid in the northern region of Drake Passage. US2 and US5 are the only DIMES expeditions to survey the Drake Passage region, which we define as the region between Cape Horn and the Antarctic Peninsula. In this region the various fronts of the Antarctic Circumpolar Current (ACC) are often compressed to the northern half of the Passage, enhancing the flow over the dramatic seafloor topography of the region.

The US2 expedition, on the R/V *Thomas G. Thompson* during January–March 2010, was the most expansive of the DIMES surveys, occupying a survey grid over a nearly 10^6-km^2 region of the eastern Pacific sector of the Southern Ocean, as well as a section across the Phoenix Ridge of Drake Passage. A description of the US2 study and a discussion of the US2 data have been previously presented by Ledwell et al. (2011) and St. Laurent et al. (2012). The US5 expedition, on the research vessel icebreaker (RVIB) *Nathaniel B. Palmer* between October

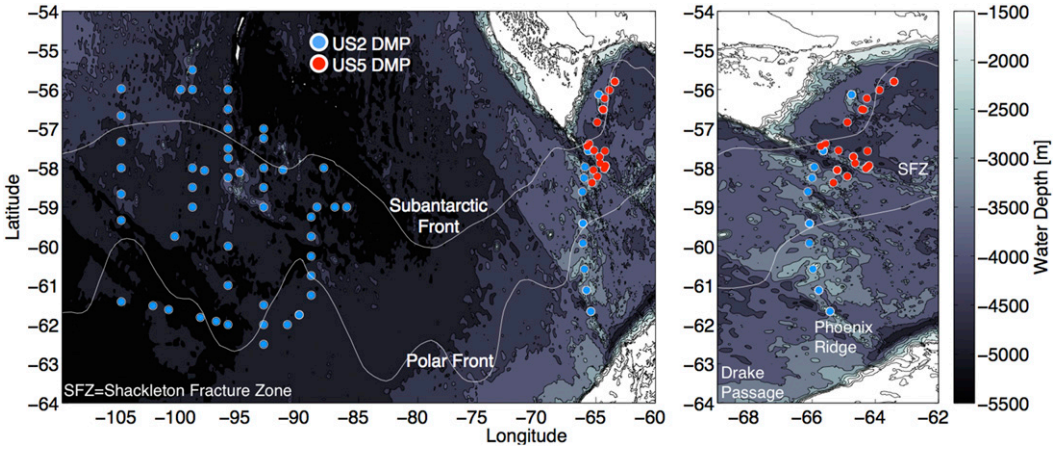

FIG. 1. Map showing the microstructure stations taken during the US2 (blue) and US5 (red) cruises. The gray contours show water depth from Smith and Sandwell (1997). The white lines represent the climatological location of the Subantarctic and Polar Fronts, from Orsi et al. (1995).

and November 2013, was the first DIMES measurement program done during austral spring. The survey grid was situated over the Subantarctic Front and Polar Front regions, downstream of the Phoenix Ridge and extending over the seafloor topography of the Shackleton Fracture Zone.

Each cruise included fine- and microstructure profiling, CTD hydrographic measurements, and ship and lowered acoustic Doppler current profiling (SADCP and LADCP) of the oceanic velocity structure. Velocity measurements from two instruments, a 300-kHz LADCP and a modular acoustic velocity sensor (MAVS), which is part of the High Resolution Profiler 2 (HRP2) package, were used in this study. The LADCP was mounted on the CTD rosette package, which was lowered using a cable winch system. A subset of the profiles was collocated and concurrent to microstructure measurements from the free-falling profiler.

Measurements of velocity microstructure (reported here in terms of the dissipation rate of turbulent kinetic energy) were acquired at a total of 88 discrete stations: 15 stations in Drake Passage along the Phoenix Ridge (US2), 23 in the Shackleton Fracture Zone (US5), and 50 stations in the upstream region of the eastern Pacific (US2), as shown in Fig. 1. During the US2 survey, two profiling instrument systems were used: the HRP2, built at Woods Hole Oceanographic Institution, and the Rockland Vertical Microstructure Profiler (VMP) 6000 (RVMP), manufactured by Rockland Scientific International, Inc. (http://www.rocklandscientific.com). During the US5 survey, only the RVMP was operated. HRP2 is similar to the original HRP (Schmitt et al. 1988).

Both instruments measure centimeter-scale shear and temperature from which ε and χ can be estimated. Additionally, the profilers have CTDs for measurements of temperature and salinity. Microstructure variance is estimated using spectral analysis over 1-m depth intervals of each profile record using methods well described in the literature (e.g., Schmitt et al. 1988; Gregg 1999; Lueck et al. 2002). No spectral corrections are done to the shear spectra, as the inertial subrange and dissipative roll-off were always well resolved. The thermal gradient spectra are well resolved out to about 20 Hz, and issues with estimating χ are described by Gregg (1999) and Nash and Moum (1999). To account for unresolved thermal variance in the diffusive subrange, we match the variance of the resolved portion of the measured temperature spectrum ($f < 20$ Hz) to that of the Batchelor model (Batchelor 1959; Oakey 1982) corresponding to our measured value of ε. Further details on the estimation of χ are given in the appendix. The RVMP uses dual shear and thermistor probes, while the HRP2 uses two shear probes, one thermistor, and one dual-needle microconductivity sensor. The dissipation rates reported are typically the mean of the independently estimated dissipation rates from each probe.

3. Analysis

a. *Water mass variability and T/S intrusions*

Water mass variability in the study region is high, as illustrated by hydrographic profiles from two stations in northern Drake Passage separated by <14 km. The two profiles were collected on separate cruises between the Polar and Subantarctic Fronts and shed light on seasonal variability (Fig. 2a). Interleaving patterns in temperature (Fig. 2b) and salinity (Fig. 2c) are characteristic of the upper 200–1000 m throughout the region. These features are density compensated and supported by mesoscale eddy activity and water mass variability. The

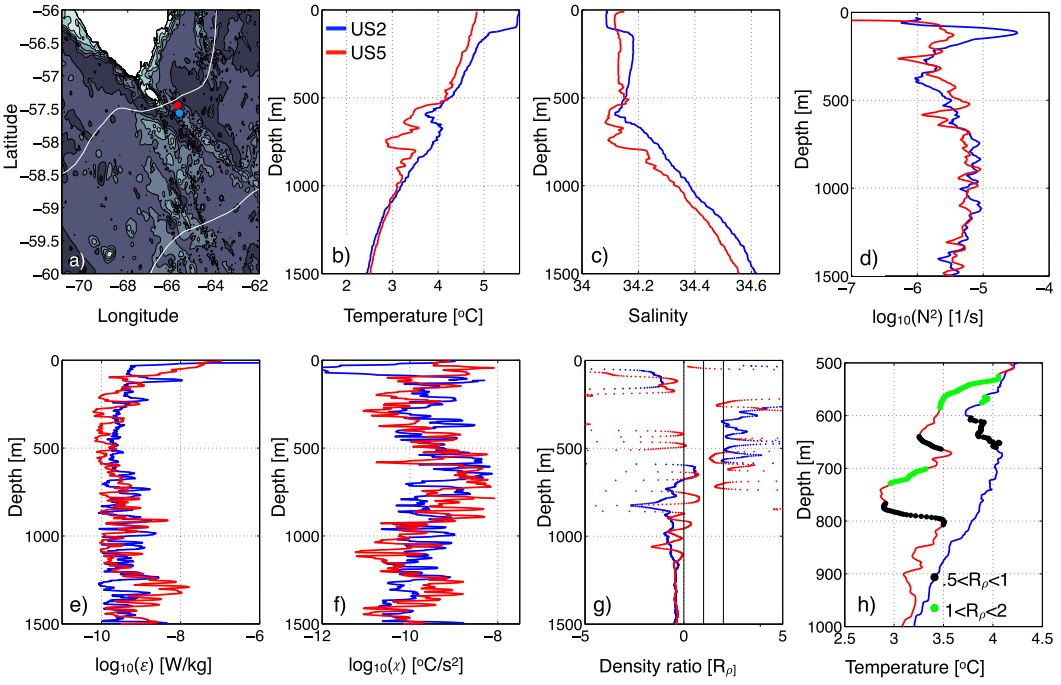

FIG. 2. (a) Blue (US2, January–March 2010) and red (US5, October–November 2013) stations within 14 km of each other. Profiles of (b) temperature and (c) salinity show evidence of intrusive behavior between 300 and 1000 m. (d) The stratification is similar in each season, with the exception of a peak at the base of the mixed layer in austral summer (December–March). Turbulent dissipation rates (e) ε and (f) χ show similar seasonal characteristics in magnitude and depth structure; χ is enhanced in the regions of strong T/S interleaving. (g) The density ratio R_ρ shows values in the intrusive region of the water column consistent with both diffusive convection and salt fingering. (h) A closer look at the temperature profiles shows regions where diffusive convection is likely occurring (black), and similarly for salt fingering (green).

buoyancy frequency (Fig. 2d) peaks at the base of the mixed layer in US2, whereas the water column is weakly stratified during US5. Shallow mixed layers (<100 m) in the region are characteristic of austral summer (Dong et al. 2008). The water masses that contribute to the intrusive behavior in the upper 1000 m are Antarctic Surface Water (ASW), Upper Circumpolar Deep Water (UCDW), Winter Water (WW), and Antarctic Intermediate Water (AAIW).

The dissipation rate of turbulent kinetic energy (Fig. 2e) is elevated in the near surface and decays to background levels between 200 and 1000 m. We attribute higher values of ε near 1500 m, particularly during US5, to breaking internal waves that were generated at the seafloor. In contrast, the dissipation rate of thermal variance χ (Fig. 2f) is enhanced at middepth, in the same depth range as strong T/S intrusions. The highest values are found between 400 and 800 m. The density ratio for the two profiles shown in Fig. 2g is computed using a 50-m depth interval for the vertical gradients of T and S. Based on the density ratio, we identify depth ranges in the temperature profile (Fig. 2h) that are favorable to salt fingering ($1 < R_\rho < 2$) and diffusive convection ($0.5 < R_\rho < 1$). The ranges of R_ρ chosen correspond to growth rates that exceed the buoyancy period (Schmitt 1994). The regions identified in Fig. 2h correspond to enhanced values of χ in Fig. 2f.

b. *Turbulent quantities in the upper 1500 m*

Mean estimates of the dissipation rates ε and χ are shown in Fig. 3 (left) and (right), respectively. The profiles are averaged in 100-m depth bins where the upper 200 m are excluded to remove mixed layer and transition layer effects (Sun et al. 2013). The shaded region represents the 95% confidence interval using a bootstrap method where the degrees of freedom are equal to the number of 10-m intervals in each bin. The 10-m length scale is chosen as an approximate value of the Ozmidov scale $L_o = \sqrt{\varepsilon/N^3}$, the eddy-overturning length scale in a stratified flow.

The average rates of turbulent kinetic energy dissipation range from $10^{-10}\,\mathrm{W\,kg^{-1}}$ upstream to $5 \times 10^{-10}\,\mathrm{W\,kg^{-1}}$ in Drake Passage. Mixing rates taken during the US5 cruise are higher at all depths between 200 and 1500 m, suggestive of a seasonal difference between austral summer (US2) and spring (US5).

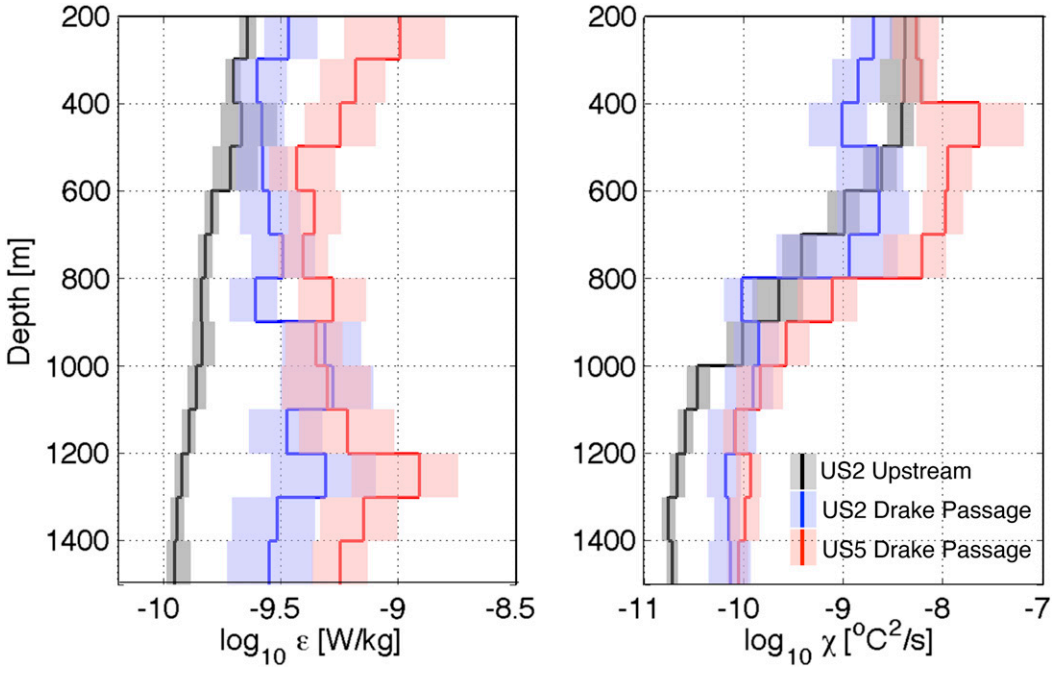

FIG. 3. Averaged (left) ε and (right) χ as a function of depth. The colors represent different subsets of the data: US2 is split into upstream (southeast Pacific) stations (black) and stations in Drake Passage (blue). Data from US5 are shown in red. The shaded regions represent error bars using a bootstrap method. The upper 200 m are not shown to remove the mixed layer and transition layer signal where stratification is highly variable and surface forcing has a significant impact. Averages are computed in 100-m bins with stations whose bottom depth was shallower than 2000 m removed.

However, it is noted that US5 was concentrated in the Polar Front region while the US2 survey sampled farther south in Drake Passage. All mixing rates in Drake Passage, including those from US2, are higher in this depth range than those taken upstream. This is likely because of topographic roughness and convergence of the frontal jets in Drake Passage that support lee wave activity and enhance the internal wave field at middepth. The thermal variance dissipation rate is enhanced between 200 and 1000 m, with the largest values occurring in the US5 survey, which was primarily conducted in the Subantarctic Front and Polar Front. The large water mass variability in this region preconditions the water column for double-diffusive instabilities.

c. *Statistics of dissipation at middepth sorted by density ratio and Richardson number*

To study the relationship between double-diffusive instability and the dissipation rates ε and χ, histograms of each are examined relative to the Richardson number and the density ratio. Only data in the depth range of 200–1000 m are used for this analysis. This eliminates surface and bottom-boundary-layer effects and isolates the signal associated with intrusive T/S features. The Richardson number is defined as $\mathrm{Ri} = N^2/(\mathrm{Sh}^2)$ where $\mathrm{Sh}^2 = \partial u^2/\partial z + \partial v^2/\partial z$. Low Ri (<0.25) is a necessary condition for (linear) shear instability resulting in turbulence and mixing. The probability density functions (PDFs) of ε and χ are sorted by the Richardson number Ri and density ratio R_ρ (Fig. 4). Statistics are calculated using the subset of microstructure profiles from the HRP2 because of the high-vertical-resolution velocity measurement from the MAVS. The Richardson number is computed over 10-m intervals to represent the Ozmidov scale. The density ratio R_ρ is computed from averages over 50-m intervals. Stable density ratios (blue histograms) are associated with low values of χ at all values of the Richardson number. The histograms of ε show no significant trend when binned by the density ratio. The levels of χ are higher for values of $\mathrm{Ri} > 0.25$ and R_ρ in the range favorable to both diffusive convection and salt fingering. These patterns suggest that double-diffusive instabilities may be more important for mixing in the 500–1000-m depth range than shear instabilities. We will explore this possibility in section 3d in the context of vertical diffusivities.

d. *Methods of estimating vertical diffusivity*

Vertical diffusivity estimates typically invoke the Osborn (1980) method, which is based on an energetic argument that steady-state, ensemble-averaged flow is in balance as $\langle P \rangle = \langle \varepsilon \rangle + \langle J_b \rangle$, where P stands for production of turbulent kinetic energy by the Reynolds

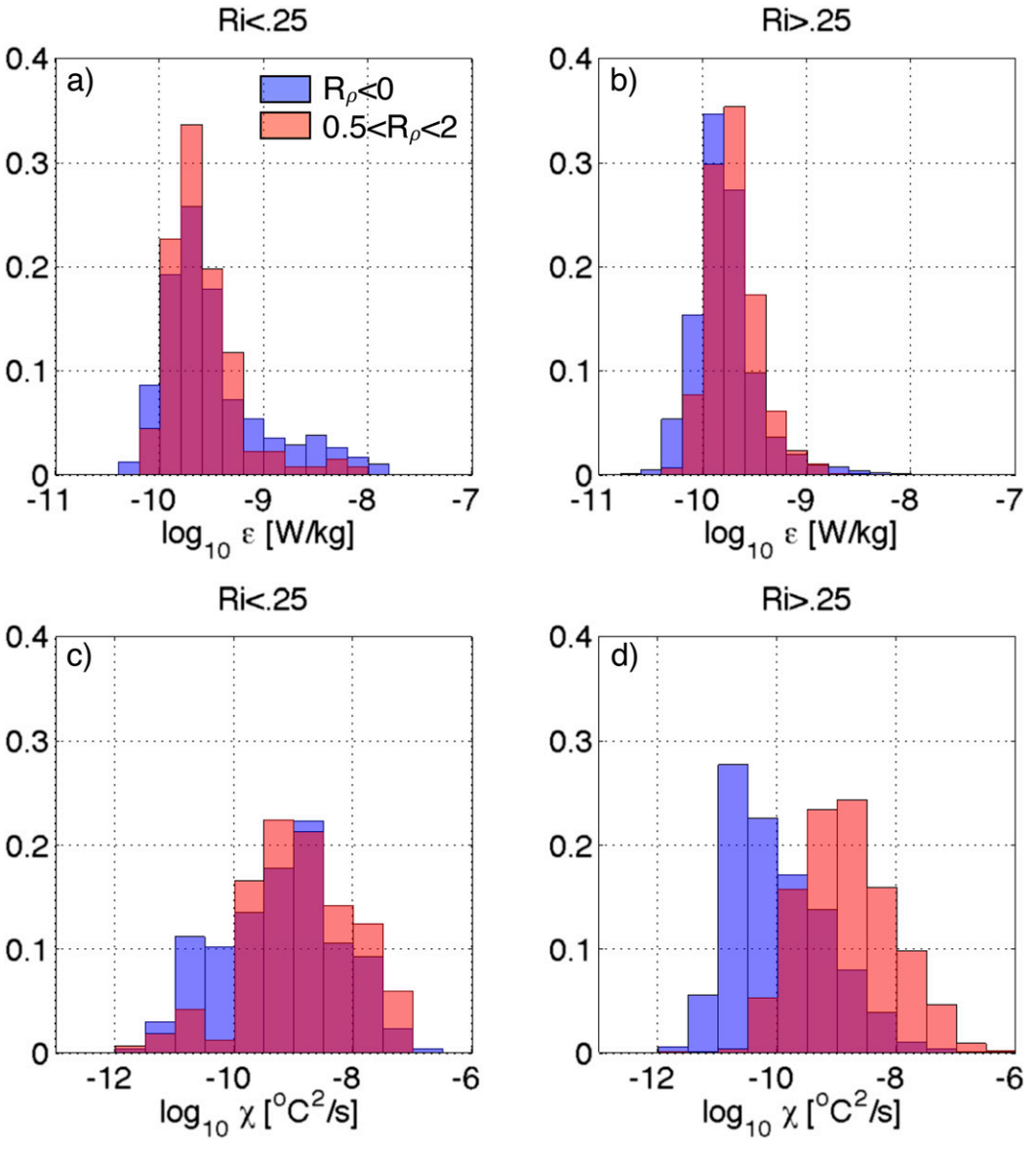

FIG. 4. PDFs of (a),(b) ε and (c),(d) χ between 200 and 1000 m are sorted by density ratio and Richardson number. Statistics in blue represent a stable density ratio ($R_\rho < 0$), and those in red represent a regime strongly susceptible to diffusive convection and salt fingering ($0.5 < R_\rho < 2$). Statistics of ε are similar for all values of R_ρ. PDFs show preference to high values of χ for R_ρ in the double diffusive regime. The darkest color indicates where the probability density functions overlap.

stresses acting on the mean background shear. The viscous dissipation rate of turbulent kinetic energy ε and the increase in mean potential energy by the turbulent buoyancy flux J_b represent two sinks of energy. Assuming a downgradient eddy diffusion parameterization yields the vertical diffusivity

$$\kappa_\rho = \frac{\Gamma^{(t)}\langle\varepsilon\rangle}{\langle N^2\rangle}, \tag{1}$$

where $\Gamma^{(t)}$ is the ratio of potential energy gain to turbulent kinetic energy loss. This term is related to the mixing efficiency of turbulence and the scaled ratio of χ to ε (see below), and $\Gamma^{(t)}$ is often taken as a constant value of 0.2. The averaging operations represented by $\langle\cdot\rangle$ are ensembles over many turbulent patches. A comprehensive discussion of these concepts is presented by St. Laurent and Schmitt (1999) and others.

The Osborn and Cox (1972) method gives an alternate way of estimating vertical diffusivity based on the rate of

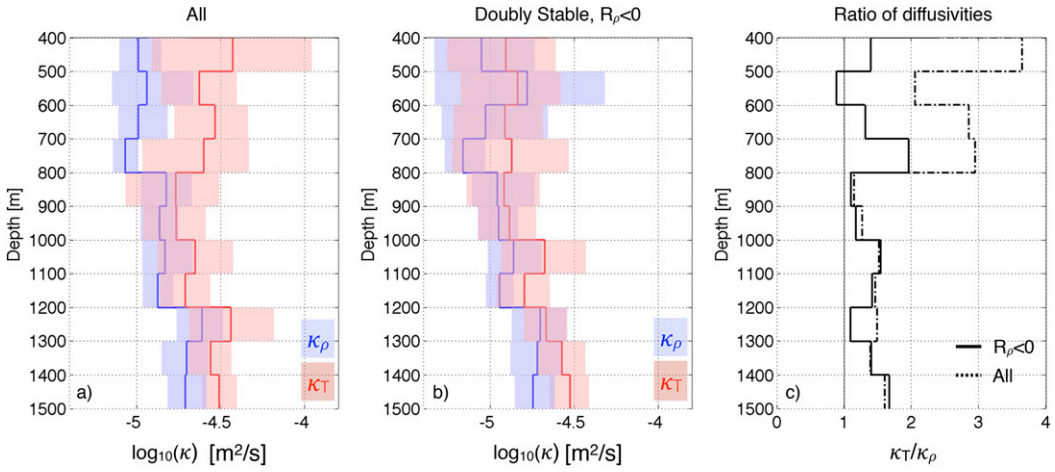

FIG. 5. Diffusivity as a function of depth computed using (a) all data during the two expeditions and (b) only data in the doubly stable regime, where $R_\rho < 0$. The data are averaged in 100-m bins using the Osborn (1980) method (κ_ρ, blue) and the Osborn and Cox (1972) method (κ_T, red). In the depth range associated with *T*/*S* intrusions (400–800 m), the values of κ_T exceed κ_ρ when all data are used. When data in the intrusive regime but with a doubly stable density ratio are used to compute diffusivity, this signal is eliminated and $\kappa_T \approx \kappa_\rho$. (c) The ratio of κ_T/κ_ρ as a function of depth is shown for the doubly stable regime (solid) and all data (dashed).

molecular diffusion of scalar variance. The scalar in this study is temperature. The fundamental assumption in this method is that at the scale relevant to the estimation of χ, the vertical fluxes dominate the variance production. Using a downgradient eddy diffusion parameterization as in the Osborn (1980) method, diffusivity is estimated as

$$\kappa_T = \frac{\langle \chi \rangle}{2\left(\frac{\partial \overline{T}}{\partial z}\right)^2}. \tag{2}$$

Using both methods and direct measurements of the turbulent quantities ε and χ, vertical diffusivity is evaluated as a function of depth. The mean estimates are computed in 100-m bins shown in Fig. 5, with blue curves for κ_ρ and red curves for κ_T. The shaded regions represent the 95% confidence intervals based on a bootstrap method where the degrees of freedom are set by the number of 20-m segments in each bin (a conservative estimate of degrees of freedom based on the larger estimates of the Ozmidov scale). Diffusivity is computed using all data from both expeditions (Fig. 5a) and the subset of data with a doubly stable density ratio ($R_\rho < 0$; Fig. 5b). The values of ε, χ, T_z, and N^2 are taken as ensemble averages over each 100-m bin. To strengthen the criterion for doubly stable statistics, the density ratio R_ρ for that subset of the data was required to be less than zero on scales of 2, 5, 10, and 25 m. This eliminates the subjective nature of classifying a hydrographic segment based on scale-dependent gradients. To represent the enhanced temperature gradients associated with intrusions of various vertical scales, the 100-m ensemble averages of $\overline{T}_z$ are composed of gradients over scales of 5 m.

In the region where *T*/*S* intrusions are prevalent, the values of κ_T exceed those of κ_ρ. Where there is no intrusive behavior notably at depths below 800m, $\kappa_T \approx \kappa_\rho$ (Fig. 5c). If shear-driven turbulence is dominant, it is expected that the two methods for computing diffusivity will produce equal values. However, in the case of double-diffusive instability contributing to turbulent mixing, the Osborn (1980) model fails, as the concept of mixing efficiency becomes ill defined (St. Laurent and Schmitt 1999). Thus, the Osborn and Cox (1972) method provides the reliable means for estimating diffusivity for double-diffusive scenarios. This is validated further by the result that $\kappa_T \approx \kappa_\rho$ for data in the intrusive depth range but with doubly stable density ratio (Fig. 5b). This is consistent with Stern et al. (2001), who showed that for Richardson numbers >0.5, salt fingers are resilient to shear processes. For this subset of the data, the mesoscale eddy field is active, the water column is not susceptible to double diffusion, and the two methods for computing diffusivity yield the same value. The ratio of κ_T to κ_ρ (Fig. 5c) for all data (dashed) show that κ_T exceeds κ_ρ by a factor of 3 in the intrusive regime. The ratio of diffusivities for the doubly stable data (solid) is less than 1.5 and converges with the ratio for all data below the intrusive regime (>800 m).

e. Spatial patterns in intrusive regions

It has been shown using direct measurements that the dissipation rate of thermal variance is enhanced in intrusive

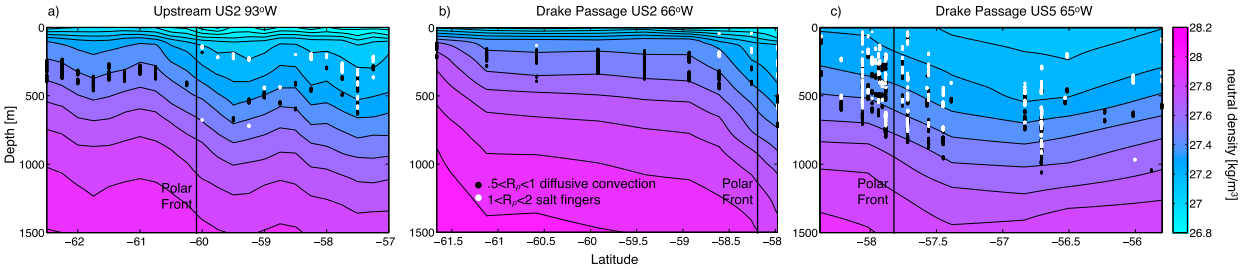

FIG. 6. Three meridional transects of neutral density (colors) at (a) 93°W, (b) 66°W, and (c) 65°W. The circles represent regions in the water column where the density ratio R_ρ is between 0.5 and 1 (black) and 1 and 2 (white). These ranges represent potential for double-diffusive instabilities with growth rates comparable to the buoyancy frequency (N), the time scale associated with internal-wave-driven turbulence. The density ratio is preferable to double-diffusive instability in neutral density classes between 27.2 and 27.7 kg m^{-3}. The PF in each panel is defined by the hydrographic measurements made during the respective cruises, (a),(b) US2 and (c)US5.

regions of the water column. With limited measurements from microstructure profilers, hydrographic data are used to study large-scale spatial patterns of the density ratio in this region. Using temperature and salinity data from CTD casts, the density ratio is computed in 50-m depth intervals for three meridional sections at 93°W (Fig. 6a) and in the Drake Passage (Figs. 6b,c).

The region of the water column susceptible to double diffusive instability corresponds to density classes between 27.2 and 27.7 kg m^{-3}. South of the Polar Front, the density ratio is predominately in the range favoring diffusive convection. North of the PF and in the frontal region, salt fingering becomes more prevalent. This pattern south of the PF is likely due to the temperature inversion that exists between 100 and 300 m as winter water subducts. Because the isopycnals deepen from south to north through Drake Passage, the potential for double diffusion extends deeper into the water column in the Polar Front and Subantarctic Front.

4. Discussion

It has been difficult to assess values and patterns of subsurface mixing because of a lack of direct observations in the Southern Ocean. Turbulent quantities are important to the energy balance of the global ocean and are prevalently parameterized in large-scale circulation models. Results from previous work using fine-structure methods to interpret mixing rates have recently been shown to be biased high (Frants et al. 2013; Mater et al. 2015; Waterman et al. 2014), often by up to two orders of magnitude. This work has revisited the values and patterns of middepth mixing in this region to inform modeling efforts and large-scale estimates of vertical diffusivity. Even with double-diffusive enhancement of κ_T relative to κ_ρ, our estimates are still typically an order of magnitude less than values of diffusivity estimated from fine-structure methods.

Intrusive features in the water column are associated with statistics of ε and χ that, when sorted by the density ratio and Richardson number, show a prevalence toward high values of χ for Ri > 1 and $0.5 < R_\rho < 2$. This corresponds to the highly double-diffusive-favorable regime described by Schmitt (1994) and St. Laurent and Schmitt (1999), where double-diffusive growth rates are comparable to the local buoyancy frequency. The potentially important role of double-diffusive processes in enhancing mixing rates has long been suggested for this region of the Southern Ocean (Joyce et al. 1978; Toole and Georgi 1981; Thompson et al. 2007).

To study interactions between the large, intermediate, and dissipative scale, we consider the triple decomposition, proposed by Stern (1967). This approach has been used in various forms by other investigators (Joyce 1977; Davis 1994; Garrett 2001; Ferrari and Polzin 2005). Here, we use the formulation of Joyce (1977), who specifically considered the case of intrusions occupying the intermediate scale between the large-scale mean (dominated by eddies) and the turbulent scale where dissipation occurs. The velocity and temperature parameters are taken to be the sum of contributions from the three scales: $\phi = \overline{\phi} + \tilde{\phi} + \phi'$, where the $\overline{(\cdot)}$, $\widetilde{(\cdot)}$, and $(\cdot)'$ denote the large, intrusive, and dissipative scales, respectively. The statistics on these disparate scales are assumed to be uncorrelated such that averaging operations obey $\overline{\tilde{\phi}} = \tilde{\phi}' = 0$. This particular assumption is equivalent to asserting there is a spectral gap between the classes of processes involved, which is impossible to justify formally. As discussed by Davis (1994), the value of the triple decomposition may be more pedagogical than literal. Here, we present the formulation of thermal variance to establish a framework connecting the dissipative processes to the larger-scale system of the Southern Ocean.

Under these assumptions, the steady-state, nondivergent thermal variance balances connecting the intermediate

to the large scale, and the small to the intermediate scale, become

$$\langle \tilde{\mathbf{u}}\tilde{T}\rangle \cdot \nabla\overline{T} - \langle \widetilde{\mathbf{u}'T'} \cdot \nabla\tilde{T}\rangle = 0 \quad \text{and} \tag{3}$$

$$\langle \widetilde{\mathbf{u}'T'} \cdot \nabla\tilde{T}\rangle + \langle \mathbf{u}'T'\rangle \cdot \nabla\overline{T} = -\frac{1}{2}\langle\chi\rangle, \tag{4}$$

where vector $\mathbf{u}$ is the velocity, $\widetilde{(\cdot)}$ represents an ensemble average over scales that are large compared to the dissipative scale and small compared to the intermediate scale, and $\langle\cdot\rangle$ represents an ensemble average over scales that are large compared to the intermediate scale and small compared to the large scale. Ferrari and Polzin (2005) employ these same equations but label the intermediate scale as being attributable to mesoscale eddies rather than intrusions. The representation of intrusions as the intermediate scale is consistent with the original formulations of Stern (1967) and Joyce (1977). Joyce (1977) specifically discussed (3) in the context of the variance production of the intrusive scale balancing that of the larger scale. Substituting (3) into (4) gives

$$\langle \tilde{\mathbf{u}}\tilde{T}\rangle \cdot \nabla\overline{T} + \langle \mathbf{u}'T'\rangle \cdot \nabla\overline{T} = -\frac{\langle\chi\rangle}{2}. \tag{5}$$

As described by Ferrari and Polzin (2005), it is conventional to represent the terms on the left-hand side as diffusion terms. The first term, representing the variance production of intermediate scale, is taken as a lateral (isopycnal) eddy flux acting on the lateral temperature gradient, such that $\langle \tilde{\mathbf{u}}\tilde{T}\rangle \cdot \nabla_{\text{iso}}\overline{T} = -K_e|\nabla\overline{T}|^2$, where K_e represents a diffusivity for eddy stirring. The second term, representing the variance production by the turbulent scale, is taken as a vertical (diapycnal) turbulent flux acting on the vertical temperature gradient, such that $\langle \mathbf{u}'T'\rangle \cdot \nabla\overline{T} = -\kappa_T\overline{T}_z^2$. Used in (5), these give

$$K_e|\nabla_{\text{iso}}\overline{T}|^2 + \kappa_T\overline{T}_z^2 = \frac{\langle\chi\rangle}{2}. \tag{6}$$

This expression may be thought of as a generalized version of the Osborn and Cox (1972) relation (2), with the thermal variance production now being shared by the intermediate scale, as represented by the K_e term, and the turbulent scale. Barring some additional information, it is not possible to calculate the diffusivity parameters (K_e, κ_T) in (6) from measured data. Notably, this study shows that replacing κ_ρ from (1) with κ_T is not an acceptable choice in an intrusive water mass where double-diffusive processes are active. Alternatively, if independent estimates of K_e are available, they could be used in (6) to estimate κ_T from estimates of $\langle\chi\rangle$. Lacking such additional information the problem is underdetermined, so we study the limits of the balance by evaluating the upper bound of each term separately. For this assessment, we will use data from US5, as it comes from a small region of the frontal zone where the hydrography does not vary widely by latitude, and the sample grid allows us to estimate lateral gradients on the mesoscale.

First, we study the limit where the K_e term can be neglected in (6) and estimate κ_T. As an alternative to the estimates presented in the previous section, we base our estimates here using the scale of the intrusions as defining the vertical scale (typically 50–100 m) for the estimates of $\overline{T}_z$. We also estimate the buoyancy gradient N^2 for use in comparative estimates of κ_ρ from (1). To accurately estimate vertical gradients in the intrusions, the density is sorted to the minimum potential energy state (Winters and D'Asaro 1996) over each intrusion. This removes any bias incurred by an arbitrary choice of vertical scale. The vertical gradient of temperature is done as a linear regression. The ensemble average is done over 0.05 kg m^{-3} bins of neutral density, and the resulting κ_ρ and κ_T estimates are given in Fig. 7. Error bars are consistent with bootstrap estimates from Fig. 5. Data are used from US5 in the density bins associated with intrusions with criteria that the intrusions are at least 5 m in length and that the density ratio is in the range of $0.5 < R_\rho < 2$. This isolates the signal in the intrusive regime of features that are potentially doubly diffusive. In this range, $\kappa_T > \kappa_\rho$ further corroborating the evidence that double-diffusive instabilities are contributing to enhanced levels of diapycnal diffusivity.

Next, we study the limit of the maximum potential role of eddy stirring in supporting thermal variance production by neglecting the κ_T term in (6) and estimating K_e. This gives

$$K_e \sim \frac{\langle\chi\rangle}{\langle 2|\nabla_{\text{iso}}\overline{T}|^2\rangle}. \tag{7}$$

Using (7) with objectively mapped isopycnal temperature gradients from the US5 dataset over scales greater than 100 km, we estimated the parameter K_e as shown in Fig. 8. The values inferred by (7) are $O(10^3$–$10^4)$ m^2 s^{-1} in the intrusive regime.

Our estimates of K_e are an upper bound, representing the limit where the variance budget is closed between mesoscale stirring along isopycnals and the thermal variance dissipation. This is extremely unlikely, as variance production by vertical mixing must play a role. To assess the relative role of eddy stirring relative to vertical mixing, we consider previous estimates of K_e from modeling studies. High-resolution modeling of the ACC system has been considered by a number of investigators (Abernathey et al. 2010; Ferrari and Nikurashin 2010;

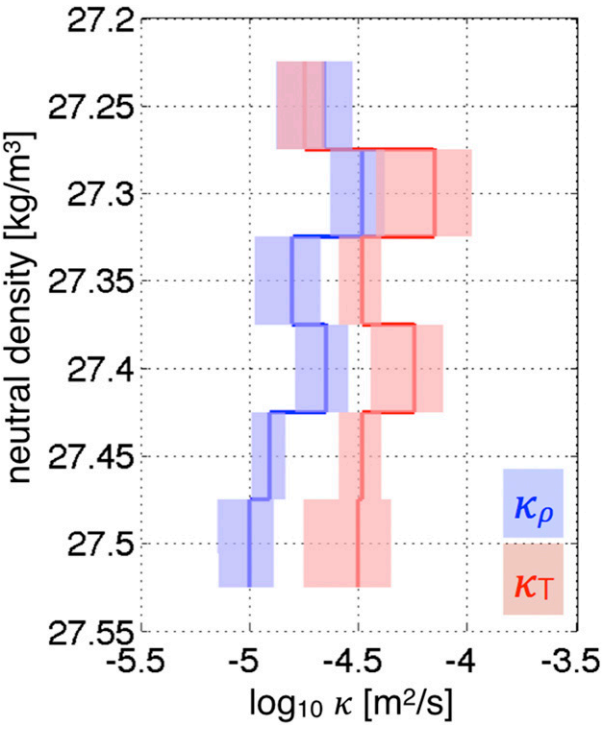

FIG. 7. The values of κ_ρ (blue) and κ_T (red) in 0.05 kg m^{-3} neutral density bins using the US5 dataset. A linear regression over each intrusion is used to compute values of $|T_z|$ and N^2. The density is first sorted to the minimum potential energy state before calculating the buoyancy frequency. Only bins of neutral density γ that included intrusions are shown, and the values of κ_T and κ_ρ are computed using intrusion-scale quantities averaged in each bin. Additionally, only intrusions that satisfy the criterion of $0.5 < R_\rho < 2$ are shown in order to isolate the signal of features that are potentially doubly diffusive.

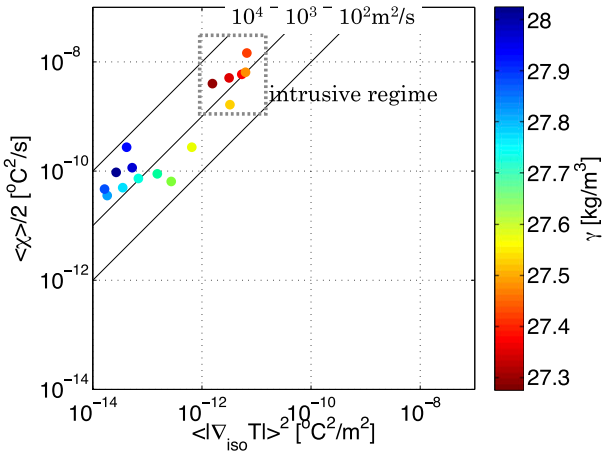

FIG. 8. Ensemble averages in 0.05 kg m^{-3} neutral density bins are taken of $\langle\chi\rangle/2$ and $\langle|\nabla_{\rm iso}T|\rangle^2$ to study the limit of the thermal variance budget where vertical dissipation is neglected. In this limit, the value of K_e, taken as upper bound, is generally larger than 10^3 m^2 s^{-1}. The black lines represent lines of constant K_e of 10^2, 10^3, and 10^4 m^2 s^{-1}.

Klocker and Abernathey 2014). Estimates for the general ACC system show K_e in the range $O(10^2$–$10^3)$ m^2 s^{-1}. Ferrari and Nikurashin (2010) specifically considered the case of eddy stirring in the frontal jet of the ACC, describing suppression of K_e values in the core of the frontal zone. There, values of K_e are predicted to be $O(10^1$–$10^2)$ m^2 s^{-1}. Recently, Naveira Garabato et al. (2016) used data-based estimates, showing K_e values of $O(10^1)$ m^2 s^{-1} in the core of the frontal zone just east of Drake Passage, further supporting the suppression of isopycnal stirring in the upper 1000 m of the frontal zones in this region.

Data from the US5 expedition used in this study was taken in the Subantarctic Front and Polar Front, such that suppressed levels of eddy mixing described by Ferrari and Nikurashin (2010) and Naveira Garabato et al. (2016) are expected. Thus, our estimates from (7) are seemingly $O(2$–$3)$ times larger than these studies suggest for the eddies in this region. This suggests that the variance production necessary to support our observations of $\langle\chi\rangle$ must predominantly come from vertical mixing, suggesting

$$\frac{2\kappa_T\overline{T}_z^2}{\langle\chi\rangle} \approx 1 + O(10^{-2}). \tag{8}$$

In this statement, the impact of the intrusive water mass is crucial for elevating κ_T relative to mixing levels that would occur in the absence of double diffusion. If double diffusive instability is driving enhanced dissipation in the intrusive layers, the mixing efficiency of $\Gamma^{(t)} = 0.2$ used in the Osborn (1980) model is invalid. To assess the failure of the mixing efficiency model in the intrusive water mass, we estimate the dissipation ratio,

$$\Gamma = \frac{\langle\chi\rangle\langle N^2\rangle}{2\langle\varepsilon\rangle\langle T_z\rangle^2}. \tag{9}$$

In the case of turbulent mixing, the dissipation ratio is related to the mixing efficiency of turbulence and generally has a value of $\Gamma = \Gamma^{(t)} \approx 0.2$. In the case of double-diffusive-driven mixing, the dissipation ratio elevates, typically to values between 0.5 and 1 (St. Laurent and Schmitt 1999). It follows that estimates of the dissipation ratio are used to identify double-diffusive processes. The dissipation ratio for the intrusive regions of the water column in the US5 data (Fig. 9) shows elevated values of Γ consistent with double-diffusive processes. We therefore accept the Osborn and Cox (1972)–based estimate of κ_T as the most meaningful estimate of mixing rate for the intrusive water mass region.

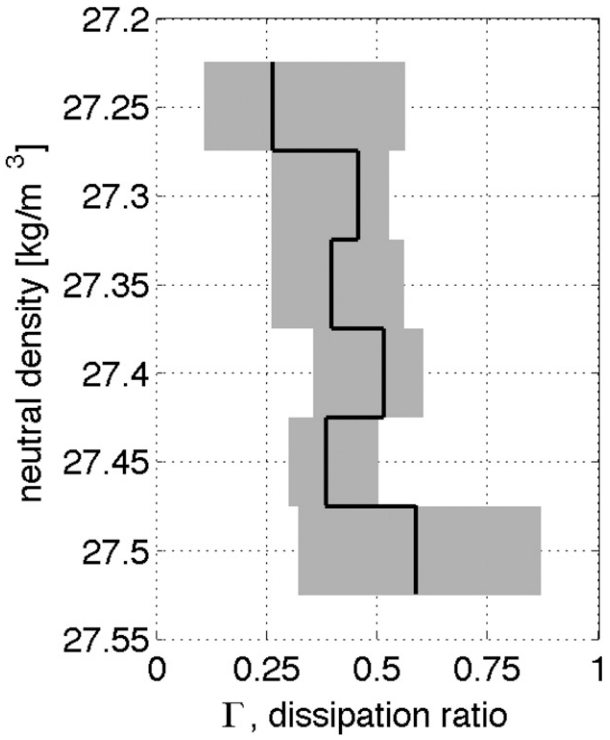

FIG. 9. Values of the dissipation ratio Γ using intrusion scale quantities that satisfy $0.5 < R_\rho < 2$. The values are consistently higher than 0.2 in the intrusive regime.

Our results indicate that it may be necessary to resolve the water mass fine structure to account for diffusive mixing in the Southern Ocean. The vertical scales of intrusions are typically in the 50–100-m range, and the gradients of temperature and salinity on these scales are the link between the mesoscale variance production and the microscale variance dissipation. While these scales are too fine to be resolved in climate models, they are resolved in global-scale process models that are used to examine the Southern Ocean (Abernathey et al. 2010; Klocker and Abernathey 2014). Our estimates of κ_T could be used to prescribe diffusivities acting in the Southern Ocean intrusive water masses of these models. Process studies with the high-resolution models could then be used to pursue parameterizations for models with coarser, non-water-mass-resolving resolutions. This approach, based on a synergy between measured data and processes-oriented numerical simulations, will likely be the most successful mechanism for parameterizing subgrid-scale physics in climate models.

The waters of the Southern Ocean have long been established to be the site of enhanced mixing. Attention has focused on the role of surface forcing, via the mixed layer, at supporting enhanced internal wave processes in the upper ocean (Dong et al. 2008; Kilbourne and Girton 2014). Even more attention has focused on the role of lee waves at driving deep turbulence levels (e.g., St. Laurent et al. 2012). At intermediate depths where intrusive water masses are present, we contend that double-diffusive processes are an important source of enhanced dissipation in this region, which generally is not accounted for in large-scale models. While estimates of mass transport are often insensitive to the particular details of how ocean processes are parameterized, the water mass characteristics of temperature and salinity can vary radically. As small changes in temperature and salinity properties evolve over long model simulation integrations, the water mass properties can diverge from reality, destroying the ability of such models to forecast thermodynamic budgets. As models will never be able to inform us of the subgrid-scale processes that drive ocean mixing, it is therefore necessary to use the data provided from direct measurements to assess the potential roles for turbulence, double diffusion, and lateral stirring.

Acknowledgments. We thank the officers and crews of the U.S. research vessels R/V *T. G. Thompson* and *N. B. Palmer* for their considerable efforts supporting the field expeditions that allowed us to collect these data. Technical staff from LDEO, WHOI, and the U.S. Antarctic Program provided heroic support of instrumentation in very challenging at-sea conditions. We additionally thank colleagues for their comments on the draft manuscript. This work was supported by grants from the U.S. National Science Foundation.

APPENDIX

Estimates and Uncertainty Associated with χ

The microstructure temperature signals are measured using FP07 probes. As described by Gregg (1999), Nash and Moum (1999), and others, these probes alias the measured signal at frequencies greater than 20 Hz. As such, a corrective method must be adopted to properly estimate temperature variance at the higher frequencies that constitute the diffusive subrange portion of the spectrum. Generally, this is done through a combination of a corrective transfer function modeled on the FP07's response and the use of a spectral model.

For our estimates, we calculate the derivative (first difference) of the microstructure temperature signal $\partial T/\partial t$ and then compute its spectrum over 2-s windows in a given profile. We then 1) correct for the first difference using a transfer function and 2) correct for probe response using the frequency response transfer function proposed by Gregg (1999) with a 5-ms time constant. We then integrate the variance of the spectrum out to

20 Hz, giving us a reference variance level. Using the known value of ε for the same spectral window, we find the Batchelor spectrum that has 1) the same value of ε and 2) the same integrated variance level to $f = 20$ Hz as the measured reference value. We then use the value of χ that goes with that Batchelor spectrum. By using the $f < 20$ Hz frequency band, we are largely insensitive to the behavior of the frequency response transfer function, but this shifts the resolution of higher-frequency variance to the spectral model of temperature fluctuations.

The assumption of a universal scalar spectrum and the estimate of the empirical scale factor q are the most significant sources of error in estimating χ. We use the Batchelor (1959) model of the temperature spectrum to account for the variance of the diffusive subrange. An alternative form of the scalar variance spectrum is presented by Kraichnan (1968). The Batchelor (1959) model with a scale factor, $q = 3.7$ (Oakey 1982), is most commonly used in the literature. A discussion of the uncertainty in q is presented by Nash and Moum (1999) and Nash and Moum (2002). A value of $q > 3.7$ gives the Batchelor spectrum more variance for a given value of χ. In the most extreme case of very high Reynolds number turbulence, Nash and Moum (2002) found half of their estimates in the range $4.2 < q < 7$, while Gargett (1985) argued q could be as large as 12. To examine the sensitivity of our χ estimates to this uncertainty, we ran calculations for both the standard value of $q = 3.7$ and the extreme value of $q = 12$. We find that for values of χ that are characteristic of our data, the larger value of q results in values of χ that are 20%–30% lower than our standard estimates. We do not believe our χ estimates are biased high, as the value of $q = 3.7$ is well established as the standard form of the Batchelor spectrum for typical oceanographic turbulence (Nash and Moum 1999). However, even in the most extreme case, uncertainty in q cannot account for the 200%–300% elevation of κ_T relative to κ_ρ in double diffusive portions of the data.

REFERENCES

Abernathey, R., J. Marshall, M. Mazloff, and E. Shuckburgh, 2010: Enhancement of mesoscale eddy stirring at steering levels in the Southern Ocean. *J. Phys. Oceanogr.*, **40**, 170–184, doi:10.1175/2009JPO4201.1.

Batchelor, G. K., 1959: Small-scale variation of convected quantities like temperature in turbulent fluid. *J. Fluid Mech.*, **5**, 113–133, doi:10.1017/S002211205900009X.

Davis, R. E., 1994: Diapycnal mixing in the ocean: Equations for large-scale budgets. *J. Phys. Oceanogr.*, **24**, 777–800, doi:10.1175/1520-0485(1994)024<0777:DMITOE>2.0.CO;2.

Dong, S., J. Sprintall, S. T. Gille, and L. Talley, 2008: Southern ocean mixed-layer depth from Argo float profiles. *J. Geophys. Res.*, **113**, C06013, doi:10.1029/2006JC004051.

Ferrari, R., and K. L. Polzin, 2005: Finescale structure of the T–S relation in the eastern North Atlantic. *J. Phys. Oceanogr.*, **35**, 1437–1454, doi:10.1175/JPO2763.1.

——, and M. Nikurashin, 2010: Suppression of eddy diffusivity across jets in the Southern Ocean. *J. Phys. Oceanogr.*, **40**, 1501–1519, doi:10.1175/2010JPO4278.1.

Frants, M., G. M. Damerell, S. T. Gille, K. J. Heywood, J. MacKinnon, and J. Sprintall, 2013: An assessment of density-based finescale methods for estimating diapycnal diffusivity in the Southern Ocean. *J. Atmos. Oceanic Technol.*, **30**, 2647–2661, doi:10.1175/JTECH-D-12-00241.1.

Garabato, A. C. N., K. L. Polzin, B. A. King, K. J. Heywood, and M. Visbeck, 2004: Widespread intense turbulent mixing in the Southern Ocean. *Science*, **303**, 210–213, doi:10.1126/science.1090929.

Gargett, A. E., 1985: Evolution of scalar spectra with the decay of turbulence in a stratified fluid. *J. Fluid Mech.*, **159**, 379–407, doi:10.1017/S0022112085003263.

Garrett, C., 2001: Stirring and mixing: What are the rate controlling processes. *From Stirring to Mixing in a Stratified Ocean: Proc. 12th 'Aha Huliko'a Hawaiian Winter Workshop*, Honolulu, HI, University of Hawai'i at Mānoa, 1–8. [Available online at http://www.soest.hawaii.edu/PubServices/2001pdfs/Garrett.pdf.]

Gregg, M., 1999: Uncertainties and limitations in measuring ε and χ. *J. Atmos. Oceanic Technol.*, **16**, 1483–1490, doi:10.1175/1520-0426(1999)016<1483:UALIMA>2.0.CO;2.

Joyce, T. M., 1977: A note on the lateral mixing of water masses. *J. Phys. Oceanogr.*, **7**, 626–629, doi:10.1175/1520-0485(1977)007<0626:ANOTLM>2.0.CO;2.

——, W. Zenk, and J. M. Toole, 1978: The anatomy of the Antarctic polar front in the Drake Passage. *J. Geophys. Res.*, **83**, 6093–6113, doi:10.1029/JC083iC12p06093.

Kilbourne, B. F., and J. B. Girton, 2014: Quantifying high-frequency wind energy flux into near-inertial motions in the Southeast Pacific. *J. Phys. Oceanogr.*, **45**, 369–386, doi:10.1175/JPO-D-14-0076.1.

Klocker, A., and R. Abernathey, 2014: Global patterns of mesoscale eddy properties and diffusivities. *J. Phys. Oceanogr.*, **44**, 1030–1046, doi:10.1175/JPO-D-13-0159.1.

Kraichnan, R. H., 1968: Small-scale structure of a scalar field convected by turbulence. *Phys. Fluids*, **11**, 945–953, doi:10.1063/1.1692063.

Kunze, E., M. G. Briscoe, and A. Williams, 1990: Interpreting shear and strain fine structure from a neutrally buoyant float. *J. Geophys. Res.*, **95**, 18 111–18 125, doi:10.1029/JC095iC10p18111.

Ledwell, J. R., L. C. St. Laurent, J. B. Girton, and J. M. Toole, 2011: Diapycnal mixing in the Antarctic Circumpolar Current. *J. Phys. Oceanogr.*, **41**, 241–246, doi:10.1175/2010JPO4557.1.

Lueck, R. G., F. Wolk, and H. Yamazaki, 2002: Oceanic velocity microstructure measurements in the 20th century. *J. Oceanogr.*, **58**, 153–174, doi:10.1023/A:1015837020019.

Mater, B. D., S. K. Venayagamoorthy, L. St. Laurent, and J. N. Moum, 2015: Biases in Thorpe-scale estimates of turbulence dissipation. Part I: Assessments from large-scale overturns in oceanographic data. *J. Phys. Oceanogr.*, **45**, 2497–2521, doi:10.1175/JPO-D-14-0128.1.

Nash, J. D., and J. N. Moum, 1999: Estimating salinity variance dissipation rate from conductivity microstructure measurements. *J. Atmos. Oceanic Technol.*, **16**, 263–274, doi:10.1175/1520-0426(1999)016<0263:ESVDRF>2.0.CO;2.

——, and ——, 2002: Microstructure estimates of turbulent salinity flux and the dissipation spectrum of salinity. *J. Phys.*

Oceanogr., **32**, 2312–2333, doi:10.1175/1520-0485(2002)032<2312:MEOTSF>2.0.CO;2.

Naveira Garabato, A. C., K. L. Polzin, R. Ferrari, J. Zika, and A. Forryan, 2016: A microscale view of mixing and overturning across the Antarctic Circumpolar Current. *J. Phys. Oceanogr.*, **46**, 233–254, doi:10.1175/JPO-D-15-0025.1.

Nikurashin, M., and R. Ferrari, 2010: Radiation and dissipation of internal waves generated by geostrophic motions impinging on small-scale topography: Application to the Southern Ocean. *J. Phys. Oceanogr.*, **40**, 2025–2042, doi:10.1175/2010JPO4315.1.

Oakey, N., 1982: Determination of the rate of dissipation of turbulent energy from simultaneous temperature and velocity shear microstructure measurements. *J. Phys. Oceanogr.*, **12**, 256–271, doi:10.1175/1520-0485(1982)012<0256:DOTROD>2.0.CO;2.

Orsi, A. H., T. Whitworth, and W. D. Nowlin, 1995: On the meridional extent and fronts of the Antarctic Circumpolar Current. *Deep-Sea Res. I*, **42**, 641–673, doi:10.1016/0967-0637(95)00021-W.

Osborn, T. R., 1980: Estimates of the local rate of vertical diffusion from dissipation measurements. *J. Phys. Oceanogr.*, **10**, 83–89, doi:10.1175/1520-0485(1980)010<0083:EOTLRO>2.0.CO;2.

——, and C. S. Cox, 1972: Oceanic fine structure. *Geophys. Astrophys. Fluid Dyn.*, **3**, 321–345, doi:10.1080/03091927208236085.

Price, J. F., 1981: Upper ocean response to a hurricane. *J. Phys. Oceanogr.*, **11**, 153–175, doi:10.1175/1520-0485(1981)011<0153:UORTAH>2.0.CO;2.

Schmitt, R. W., 1979: The growth rate of super-critical salt fingers. *Deep-Sea Res.*, **26A**, 23–40, doi:10.1016/0198-0149(79)90083-9.

——, 1994: Double diffusion in oceanography. *Annu. Rev. Fluid Mech.*, **26**, 255–285, doi:10.1146/annurev.fl.26.010194.001351.

——, J. M. Toole, R. L. Koehler, E. C. Mellinger, and K. W. Doherty, 1988: The development of a fine-and microstructure profiler. *J. Atmos. Oceanic Technol.*, **5**, 484–500, doi:10.1175/1520-0426(1988)005<0484:TDOAFA>2.0.CO;2.

Sheen, K., and Coauthors, 2014: Eddy-induced variability in Southern Ocean abyssal mixing on climatic timescales. *Nat. Geosci.*, **7**, 577–582, doi:10.1038/ngeo2200.

Sloyan, B. M., L. D. Talley, T. K. Chereskin, R. Fine, and J. Holte, 2010: Antarctic Intermediate Water and Subantarctic Mode Water formation in the southeast Pacific: The Role of turbulent mixing. *J. Phys. Oceanogr.*, **40**, 1558–1574, doi:10.1175/2010JPO4114.1.

Smith, W. H., and D. T. Sandwell, 1997: Global sea floor topography from satellite altimetry and ship depth soundings. *Science*, **277**, 1956–1962, doi:10.1126/science.277.5334.1956.

St. Laurent, L., and R. W. Schmitt, 1999: The contribution of salt fingers to vertical mixing in the North Atlantic Tracer Release Experiment. *J. Phys. Oceanogr.*, **29**, 1404–1424, doi:10.1175/1520-0485(1999)029<1404:TCOSFT>2.0.CO;2.

——, A. C. Naveira Garabato, J. R. Ledwell, A. M. Thurnherr, J. M. Toole, and A. J. Watson, 2012: Turbulence and diapycnal mixing in Drake Passage. *J. Phys. Oceanogr.*, **42**, 2143–2152, doi:10.1175/JPO-D-12-027.1.

Stern, M. E., 1967: Lateral mixing of water masses. *Deep-Sea Res. Oceanogr. Abstr.*, **14**, 747–753, doi:10.1016/S0011-7471(67)80011-1.

——, T. Radko, and J. Simeonov, 2001: Salt fingers in an unbounded thermocline. *J. Mar. Res.*, **59**, 355–390, doi:10.1357/002224001762842244.

Sun, O. M., S. R. Jayne, K. L. Polzin, B. A. Rahter, and L. C. St. Laurent, 2013: Scaling turbulent dissipation in the transition layer. *J. Phys. Oceanogr.*, **43**, 2475–2489, doi:10.1175/JPO-D-13-057.1.

Thompson, A. F., S. T. Gille, J. A. MacKinnon, and J. Sprintall, 2007: Spatial and temporal patterns of small-scale mixing in Drake Passage. *J. Phys. Oceanogr.*, **37**, 572–592, doi:10.1175/JPO3021.1.

Thorpe, S., 1977: Turbulence and mixing in a Scottish loch. *Philos. Trans. Roy. Soc. London*, **A286**, 125–181, doi:10.1098/rsta.1977.0112.

Toole, J. M., and D. T. Georgi, 1981: On the dynamics and effects of double-diffusively driven intrusions. *Prog. Oceanogr.*, **10**, 123–145, doi:10.1016/0079-6611(81)90003-3.

Waterman, S., K. L. Polzin, A. C. Naveira Garabato, K. L. Sheen, and A. Forryan, 2014: Suppression of internal wave breaking in the Antarctic Circumpolar Current near topography. *J. Phys. Oceanogr.*, **44**, 1466–1492, doi:10.1175/JPO-D-12-0154.1.

Whalen, C., L. Talley, and J. MacKinnon, 2012: Spatial and temporal variability of global ocean mixing inferred from Argo profiles. *Geophys. Res. Lett.*, **39**, L18612, doi:10.1029/2012GL053196.

Winters, K. B., and E. A. D'Asaro, 1996: Diascalar flux and the rate of fluid mixing. *J. Fluid Mech.*, **317**, 179–193, doi:10.1017/S0022112096000717.

Wu, L., Z. Jing, S. Riser, and M. Visbeck, 2011: Seasonal and spatial variations of Southern Ocean diapycnal mixing from Argo profiling floats. *Nat. Geosci.*, **4**, 363–366, doi:10.1038/ngeo1156.

You, Y., 2002: A global ocean climatological atlas of the turner angle: Implications for double-diffusion and water-mass structure. *Deep-Sea Res. I*, **49**, 2075–2093, doi:10.1016/S0967-0637(02)00099-7.